

Chiral response in two-dimensional bilayers with time-reversal symmetry: A universal criterion

Chao Ding and Mingwen Zhao ^{*}*School of Physics, Shandong University, Jinan 250100, China* (Received 28 May 2023; revised 10 August 2023; accepted 29 August 2023; published 12 September 2023)

Chiral van der Waals bilayers with interlayer quantum coupling provide an exceptional platform for manipulating the intrinsic chirality within atomically thin films. In this paper, we delve into the intrinsic chirality of two-dimensional (2D) bilayers possessing time-reversal symmetry (TRS), based on the constitutive equations and circular dichroism (CD), using the methodologies pioneered in recent works by Stauber *et al.* [*Phys. Rev. Lett.* **120**, 046801 (2018); *Phys. Rev. B* **98**, 195414 (2018)]. We introduce chiral conductivity σ_{chir} and demonstrate that $\sigma_{\text{chir}} \neq 0$ leads to a nonzero CD, unveiling the distinctive chiral response inherent in a 2D bilayer. According to the criterion, to achieve a chiral response in 2D bilayers while preserving TRS, it is essential to eliminate both mirror and spatial inversion symmetries. Through the derivation of Poynting vectors, it becomes evident that $\sigma_{\text{chir}} \neq 0$ assumes a crucial role in realizing chiral plasmons within isotropy 2D bilayers characterized by TRS in the local response limit. We also simulate the chiral response of untwisted bilayer graphene under a bias voltage by means of numerical calculations.

DOI: [10.1103/PhysRevB.108.125415](https://doi.org/10.1103/PhysRevB.108.125415)

I. INTRODUCTION

Chiral materials are abundant in nature and find extensive applications in stereochemistry [1,2], drug development [3], and spintronics [4,5] due to their unique property of being nonsuperimposable on their mirror images. Experimentally, the chirality of materials can be characterized by circular dichroism (CD), which measures the relative difference in absorption between right- and left-circularly polarized light (CPL; A_+ and A_-), $CD = (A_+ - A_-)/[2(A_+ + A_-)]$. The emergence of two-dimensional (2D) materials provides a superior platform for programming the intrinsic chirality in atomically thin films. Breaking the time-reversal symmetry (TRS) is essential to achieve chiral response in a monolayer, which makes experimental realization challenging. Here, van der Waals (VDW) bilayers offer an alternative approach for regulating the chirality by sliding or twisting between monolayers [6–10]. Twisted bilayer graphene (TBG) eliminates all mirror symmetries due to the relative rotation between two graphene layers [6,11–13]. Recent experiments show that TBG displays remarkably strong CD without the breaking TRS [14]. The CD within TBG has garnered attention from various theoretical studies [15–18], with their findings showing strong agreement with experimental observations. Transverse conductivity $\sigma_{\text{chir}} = \sigma_{xy}$ stands as a significant indicator, reflecting how current responds in one layer to an electric field perpendicular to it in another layer. It was discerned to hold the intrinsic chiral attribute responsible for the observed nonzero CD [16,17]. The chiral essence of TBG is also obtained through a tight-binding (TB) model, yielding $\sigma_{\text{chir}} = \sigma_{xy} + \sigma'_{xy}$ [19], where σ'_{xy} signifies the transverse con-

ductivity, capturing the interplay between intralayer currents and interlayer electric fields. However, for a 2D bilayer with general symmetries, such as those characterized by notable anisotropy, a broader understanding of their chiral nature becomes essential. Thus, it becomes imperative to explore the intrinsic chirality within 2D bilayer systems adhering to TRS. Such a study holds immense significance in predicting the chiral attributes of diverse 2D bilayer configurations.

Plasmons, the collective oscillations of electrons, can enhance light-matter interactions by interacting with light. This offers an efficient means of boosting chiral optical responses, such as CD [3,4,20–27], which tend to be very weak in chiral materials. Chiral Berry plasmons (CBPs) are nonreciprocal plasmon modes that are confined at the boundaries of 2D materials. Recently, they have gained significant attention [28,29] due to their ability to propagate in a strong nonreciprocal manner, providing a significant advantage in reducing energy losses. However, the creation of such a CBP is limited to materials where TRS is lifted, such as magnetic materials or gapped Dirac systems under pumping with CPL. Recently, chiral plasmons have also been discovered in TBG. The chiral plasmons in TBG are characterized by the presence of chiral electromagnetic fields, accompanied by nonzero transverse Poynting vectors [30,31]. The chiral plasmons in TBG greatly enhance the chiral response of the electromagnetic near fields, making them promising for detecting chiral molecules [30]. This finding offers a viable strategy for obtaining chiral plasmons in bilayer materials without violating TRS. However, a universal theory for the chiral plasmons in these bilayers is currently lacking, highlighting a need for further research regarding this issue.

In this paper, we delve into the intrinsic chirality exhibited by 2D bilayers adhering to TRS, based on the constitutive equations and CD, using the pioneering methodologies

^{*}zmw@sdu.edu.cn

introduced in recent works by Stauber *et al.* [16,19]. We introduce a chiral conductivity $\sigma_{\text{chir}} = \sigma_{xy} + \frac{1}{2}\sigma'_{xy} - \frac{1}{2}\sigma''_{xy}$ and demonstrate that $\sigma_{\text{chir}} \neq 0$ leads to nonzero CD and therefore features the chiral response of a 2D bilayer. We demonstrate that generation of chiral responses in bilayers requires the breaking of both mirror and spatial inversion symmetries, in sharp contrast to the case of monolayers where TRS should be lifted. In the local response limit, $\sigma_{\text{chir}} \neq 0$ is an essential requirement for the emergence of chiral plasmons within isotropic 2D bilayer with TRS. The chiral response of bilayer graphene under a bias voltage is verified by numerical calculations, which is consistent with the universal criteria.

II. CHIRAL RESPONSE IN A 2D MONOLAYER

We start from a 2D monolayer where the response of the in-plane current $\mathbf{J}(\omega)$ to the electric field $\mathbf{E}(\omega)$ is given by

$$\begin{bmatrix} J_x(\omega) \\ J_y(\omega) \end{bmatrix} = \begin{bmatrix} \sigma_{xx}(\omega) & \sigma_{xy}(\omega) \\ \sigma_{yx}(\omega) & \sigma_{yy}(\omega) \end{bmatrix} \begin{bmatrix} E_x(\omega) \\ E_y(\omega) \end{bmatrix}. \quad (1)$$

In Eq. (1), we take the long wavelength limit ($\mathbf{q} \rightarrow 0$) by assuming that the wavelength of the electric field is much larger than the lattice constant of the monolayer. The conductivity of the monolayer $\sigma_{\alpha\beta}(\omega)$ is calculated by the Kubo formula [32]:

$$\begin{aligned} \sigma_{\alpha\beta}(\omega) = & -\frac{ie^2g\hbar}{(2\pi)^2} \\ & \times \int \sum_{m,n} \frac{f_{k,m} - f_{k,n}}{\varepsilon_{k,m} - \varepsilon_{k,n}} \frac{\langle \mathbf{k}, m | v_\alpha | \mathbf{k}, n \rangle \langle \mathbf{k}, n | v_\beta | \mathbf{k}, m \rangle}{\varepsilon_{k,m} - \varepsilon_{k,n} + \hbar\omega + i\eta} \\ & \times d^2\mathbf{k}. \end{aligned} \quad (2)$$

In this expression, g is the degeneracy of the system, $\varepsilon_{k,m}$ and $|\mathbf{k}, m\rangle$ represent the energy eigenvalues and the corresponding eigenvectors, respectively, $f_{k,m}$ is the Fermi distribution function for the state with the energy of $\varepsilon_{k,m}$, and v_α is the velocity operator along the α direction. In the TB limit, the velocity operator $\mathbf{v}(\mathbf{k})$ is expressed as $\mathbf{v}(\mathbf{k}) = (1/\hbar)\nabla_{\mathbf{k}}H(\mathbf{k})$ [19], where $H(\mathbf{k})$ is the Hamiltonian matrix for wave vector \mathbf{k} . Notably, for the intraband transition ($m = n$), we have $\lim_{q \rightarrow 0}(f_{k,m} - f_{k+q,m})/(\varepsilon_{k,m} - \varepsilon_{k+q,m}) = \partial f_{k,m}/\partial \varepsilon_{k,m}$. The intraband part of conductivity $\sigma_{\alpha\beta}^{\text{intra}}(\omega)$ can be written as $\sigma_{\alpha\beta}^{\text{intra}}(\omega) = iD_{\alpha\beta}(\omega)/\omega$, where $D_{\alpha\beta}(\omega)$ is the Drude matrix elements [19].

For a monolayer, the CD can also be represented as [33]

$$\text{CD} = \frac{\text{Im}[\sigma_{yx}(\omega) - \sigma_{xy}(\omega)]}{2\text{Re}[\sigma_{xx}(\omega) + \sigma_{yy}(\omega)]}. \quad (3)$$

Obviously, a nonzero CD signal requires $\text{Im}\sigma_{yx}(\omega) \neq \text{Im}\sigma_{xy}(\omega)$. The physical meanings of this criterion are more apparent when referencing Eq. (1), which gives $(\nabla_{\mathbf{E}} \times \mathbf{J}) \cdot \mathbf{e}_z = \sigma_{yx} - \sigma_{xy}$. Here, $\sigma_{yx} - \sigma_{xy} \neq 0$ represents intrinsic spiral textures of $\mathbf{J}(\omega)$ and $\mathbf{E}(\omega)$. Therefore, we define the chiral conductivity $\sigma_{\text{chir}}(\omega) = \sigma_{yx}(\omega) - \sigma_{xy}(\omega)$, which is rotationally invariant [34], to measure the chiral response of a monolayer.

For a 2D monolayer with TRS, we have $H(\mathbf{k}) = H^*(-\mathbf{k})$ which gives the eigenvalues and eigenvectors of $\varepsilon_{k,m} = \varepsilon_{-k,m}$ and $\psi_{k,m} = \psi_{-k,m}^*$. The electron velocity given by $v_\alpha(\mathbf{k}) =$

$(1/\hbar)\partial H(\mathbf{k})/\partial \mathbf{k}_\alpha$ satisfies $v_\alpha(-\mathbf{k}) = -v_\alpha^*(\mathbf{k})$. This leads to $\sigma_{\alpha\beta}(\omega) = \sigma_{\beta\alpha}(\omega)$ according to Eq. (2). Therefore, breaking TRS is necessary for creating chiral responses with $\sigma_{xy}(\omega) \neq \sigma_{yx}(\omega)$ in a 2D monolayer [28,29]. Notably, the chiral response explored in this paper distinguishes itself from the k-resolved chiral response, which entails the selective absorption of distinct CPL by electrons in specific momentum regions (valleys). The k-resolved chiral response is observed in monolayer systems with TRS and broken inversion symmetry, such as gapped graphene and MoS₂ monolayers [35,36]. However, the total CD in these monolayer systems remains zero owing to the presence of TRS.

III. CHIRAL RESPONSE IN A 2D BILAYER WITH TRS

We divide the current $\mathbf{j}^{\text{BL}} = [\mathbf{j}^{(1)}; \mathbf{j}^{(2)}; \mathbf{j}^{(i)}]$ and electric field $\mathbf{E}^{\text{BL}} = [\mathbf{E}^{(1)}; \mathbf{E}^{(2)}; \mathbf{E}^{(i)}]$ in a 2D bilayer into three parts, where $\mathbf{j}^{(1)}$ ($\mathbf{E}^{(1)}$) and $\mathbf{j}^{(2)}$ ($\mathbf{E}^{(2)}$) are the current (or electric field) of layers 1 and 2, respectively. The interlayer current $\mathbf{j}^{(i)}$ stems from the interlayer transition of electrons. We assume that the in-plane currents are adequate to characterize the optical response [16]. Therefore, the current and electric fields are the two-component vectors and can be written as $\mathbf{j}^{(\alpha)} = [j_x^{(\alpha)}, j_y^{(\alpha)}]^T$ and $\mathbf{E}^{(\alpha)} = [E_x^{(\alpha)}, E_y^{(\alpha)}]^T$, with $\alpha \in (1, 2, i)$. Then the current \mathbf{j}^{BL} and electric field \mathbf{E}^{BL} are six-component vectors. The response for 2D bilayer becomes $\mathbf{j}^{\text{BL}} = \boldsymbol{\sigma}^{\text{BL}}\mathbf{E}^{\text{BL}}$, where the conductivity $\boldsymbol{\sigma}^{\text{BL}}$ is given by a 6×6 matrix.

For a bilayer system, the TB Hamiltonian matrix $H(\mathbf{k})$ can be partitioned into $H(\mathbf{k}) = H^{(1)}(\mathbf{k}) + H^{(2)}(\mathbf{k}) + H^{(i)}(\mathbf{k})$ corresponding to the layers of TB bases, which gives the velocity operator $\mathbf{v}^{(\alpha)} = (1/\hbar)\nabla_{\mathbf{k}}H^{(\alpha)}(\mathbf{k})$ [$\alpha \in (1, 2, i)$]. Subsequently, the conductivity $\boldsymbol{\sigma}^{\text{BL}}$ is derived based on the composite velocity vector $\mathbf{v}^{\text{BL}} = [\mathbf{v}^{(1)}, \mathbf{v}^{(2)}, \mathbf{v}^{(i)}] = [v_x^{(1)}, v_y^{(1)}, v_x^{(2)}, v_y^{(2)}, v_x^{(i)}, v_y^{(i)}]$:

$$\begin{aligned} \sigma_{\alpha\beta}^{\text{BL}}(\omega) = & -\frac{ie^2g\hbar}{(2\pi)^2} \int \sum_{m,n} \frac{f_{k,m} - f_{k,n}}{\varepsilon_{k,m} - \varepsilon_{k,n}} \\ & \times \frac{\langle \mathbf{k}, m | v_\alpha^{\text{BL}} | \mathbf{k}, n \rangle \langle \mathbf{k}, n | v_\beta^{\text{BL}} | \mathbf{k}, m \rangle}{\varepsilon_{k,m} - \varepsilon_{k,n} + \hbar\omega + i\eta} d^2\mathbf{k}. \end{aligned} \quad (4)$$

In this expression, $\alpha, \beta \in (1, 2, \dots, 6)$, and v_α^{BL} and v_β^{BL} are the α th and β th components of the composite velocity vector \mathbf{v}^{BL} , respectively. The presence of TRS leads to $\sigma_{\alpha\beta}^{\text{BL}} = \sigma_{\beta\alpha}^{\text{BL}}$. The intraband contribution of $\sigma_{\alpha\beta}^{\text{BL}}(\omega)$ relates the corresponding Drude matrix element $D_{\alpha\beta}^{\text{BL}}(\omega)$ with $\sigma_{\alpha\beta}^{\text{BL, intra}}(\omega) = iD_{\alpha\beta}^{\text{BL}}(\omega)/\omega$, which gives

$$\begin{aligned} D_{\alpha\beta}^{\text{BL}}(\omega) = & -\frac{e^2g}{(2\pi)^2} \sum_m \int \frac{\partial f_{k,m}}{\partial \varepsilon_{k,m}} \langle \mathbf{k}, m | v_\alpha^{\text{BL}} | \mathbf{k}, m \rangle \\ & \times \langle \mathbf{k}, m | v_\beta^{\text{BL}} | \mathbf{k}, m \rangle d^2\mathbf{k}. \end{aligned} \quad (5)$$

For convenience, we replace $\sigma_{\alpha\beta}^{\text{BL}}(\omega)$ and $D_{\alpha\beta}^{\text{BL}}(\omega)$ with $\sigma_{\alpha\beta}$ and $D_{\alpha\beta}$ in our subsequent discussion. We can demonstrate that only $\sigma_{14} - \sigma_{23}$, $\sigma_{16} - \sigma_{25}$, and $\sigma_{36} - \sigma_{45}$ are invariant under rotation operations and thus are available for

characterizing chiral response. Therefore, we separate the chiral part σ^{chir} from the conductivity $\sigma^{\text{BL}} = \sigma^{\text{chir}} + \sigma^{\text{achir}}$ with

$$\sigma^{\text{chir}} = \begin{pmatrix} 0 & 0 & 0 & \sigma_{xy} & 0 & \sigma'_{xy} \\ 0 & 0 & -\sigma_{xy} & 0 & -\sigma'_{xy} & 0 \\ 0 & -\sigma_{xy} & 0 & 0 & 0 & \sigma''_{xy} \\ \sigma_{xy} & 0 & 0 & 0 & -\sigma''_{xy} & 0 \\ 0 & -\sigma'_{xy} & 0 & -\sigma''_{xy} & 0 & 0 \\ \sigma'_{xy} & 0 & \sigma''_{xy} & 0 & 0 & 0 \end{pmatrix}, \quad (6)$$

and

$$\sigma^{\text{achir}} = \begin{pmatrix} \sigma_{11} & \sigma_{12} & \sigma_{13} & \tilde{\sigma}_{xy} & \sigma_{15} & \tilde{\sigma}'_{xy} \\ \sigma_{12} & \sigma_{22} & \tilde{\sigma}_{xy} & \sigma_{24} & \tilde{\sigma}'_{xy} & \sigma_{26} \\ \sigma_{13} & \tilde{\sigma}_{xy} & \sigma_{33} & \sigma_{34} & \sigma_{35} & \tilde{\sigma}''_{xy} \\ \tilde{\sigma}_{xy} & \sigma_{24} & \sigma_{34} & \sigma_{44} & \tilde{\sigma}''_{xy} & \sigma_{46} \\ \sigma_{15} & \tilde{\sigma}'_{xy} & \sigma_{35} & \tilde{\sigma}''_{xy} & \sigma_{55} & \sigma_{56} \\ \tilde{\sigma}'_{xy} & \sigma_{26} & \tilde{\sigma}''_{xy} & \sigma_{46} & \sigma_{56} & \sigma_{66} \end{pmatrix}. \quad (7)$$

In these expressions, $\sigma_{xy} = \frac{1}{2}(\sigma_{14} - \sigma_{23})$, $\sigma'_{xy} = \frac{1}{2}(\sigma_{16} - \sigma_{25})$, $\sigma''_{xy} = \frac{1}{2}(\sigma_{36} - \sigma_{45})$, $\tilde{\sigma}_{xy} = \frac{1}{2}(\sigma_{14} + \sigma_{23})$, $\tilde{\sigma}'_{xy} = \frac{1}{2}(\sigma_{16} + \sigma_{25})$, and $\tilde{\sigma}''_{xy} = \frac{1}{2}(\sigma_{36} + \sigma_{45})$. Correspondingly, we can define $D_{xy} = \frac{1}{2}(D_{14} - D_{23})$, $D'_{xy} = \frac{1}{2}(D_{16} - D_{25})$, and $D''_{xy} = \frac{1}{2}(D_{36} - D_{45})$.

To elucidate the physical significance of σ^{chir} and σ^{achir} , we adopt the assumption made in previous literature [19] that the electric field varies linearly along the z direction, which gives

$$\begin{aligned} \mathbf{E}^{(1)} &= \bar{\mathbf{E}} + \frac{1}{2}\Delta\mathbf{E}, \\ \mathbf{E}^{(2)} &= \bar{\mathbf{E}} - \frac{1}{2}\Delta\mathbf{E}, \\ \mathbf{E}^{(i)} &= \bar{\mathbf{E}}. \end{aligned} \quad (8)$$

Here, $\bar{\mathbf{E}}$ is the average electric field of layers 1 and 2, and $\Delta\mathbf{E}$ represents the difference between $\mathbf{E}^{(1)}$ and $\mathbf{E}^{(2)}$.

Then the total current $\mathbf{j} = \mathbf{j}^{\text{chir}} + \mathbf{j}^{\text{achir}}$ and difference of current between layers 1 and 2 $\Delta\mathbf{j} = \mathbf{j}^{(1)} - \mathbf{j}^{(2)} = \Delta\mathbf{j}^{\text{chir}} + \Delta\mathbf{j}^{\text{achir}}$ are obtained using the constitutive equations for σ^{chir} and σ^{achir} , which are written as

$$\begin{aligned} \mathbf{j}^{\text{achir}} &= \sigma_{j,E}^{\text{achir}} \bar{\mathbf{E}} + \frac{1}{2}\sigma_{j,\Delta E}^{\text{achir}} \Delta\mathbf{E}, \\ \Delta\mathbf{j}^{\text{achir}} &= \sigma_{\Delta j,E}^{\text{achir}} \bar{\mathbf{E}} + \frac{1}{2}\sigma_{\Delta j,\Delta E}^{\text{achir}} \Delta\mathbf{E}, \end{aligned} \quad (9)$$

and

$$\begin{aligned} \mathbf{j}^{\text{chir}} &= \frac{1}{2}\sigma_{j,\Delta E}^{\text{chir}} \Delta\mathbf{E}, \\ \Delta\mathbf{j}^{\text{chir}} &= \sigma_{\Delta j,E}^{\text{chir}} \bar{\mathbf{E}}. \end{aligned} \quad (10)$$

The response matrices $\sigma_{j,E}^{\text{achir}}$, $\sigma_{j,\Delta E}^{\text{achir}}$, $\sigma_{\Delta j,E}^{\text{achir}}$ and $\sigma_{\Delta j,\Delta E}^{\text{achir}}$ are presented in the Supplemental Material [34]. The equality of the anti-diagonal terms in these matrices provides evidence for the achiral nature of $\mathbf{j}^{\text{achir}}$ and $\Delta\mathbf{j}^{\text{achir}}$. The response matrices for chiral part of currents are

$$\sigma_{j,\Delta E}^{\text{chir}} = -\sigma_{\Delta j,E}^{\text{chir}} = -2 \begin{pmatrix} 0 & \sigma^{\text{chir}} \\ -\sigma^{\text{chir}} & 0 \end{pmatrix}, \quad (11)$$

with $\sigma^{\text{chir}} = \sigma_{xy} + \frac{1}{2}(\sigma'_{xy} - \sigma''_{xy})$. Clearly, $\sigma^{\text{chir}} \neq 0$ features a chiral response, which can be treated as a universal criterion for 2D chiral bilayers with TRS. The significance of σ_{xy} , σ'_{xy} , σ''_{xy} becomes evident when examining Eq. (6). Here, σ_{xy} represents the response of current in one layer to an electric field perpendicular to it in another layer, while σ'_{xy} (σ''_{xy}) signifies the response of current in layer 1 (2) to the interlayer electric field in the perpendicular direction. The contribution of intraband transitions to the chiral conductivity σ^{chir} can be characterized by $D_{\text{chir}} = -i\omega\sigma_{\text{chir}}^{\text{intra}}$. Therefore, we can deduce $D_{\text{chir}} = D_{xy} + \frac{1}{2}(D'_{xy} - D''_{xy})$.

Additionally, according to Maxwell's equations, we have $\mathbf{z} \times [\mathbf{E}^{(2)} - \mathbf{E}^{(1)}] = i\omega d\bar{\mathbf{B}}$, where $\bar{\mathbf{B}}$ is the averaged in-plane magnetic field component between the two layers, and d is the interlayer distance of the bilayer. Equation (10) can be written to

$$\begin{aligned} \mathbf{j}^{\text{chir}} &= -i\omega d\sigma^{\text{chir}}\bar{\mathbf{B}}, \\ \mathbf{m}^{\text{chir}} &= -d\sigma^{\text{chir}}\bar{\mathbf{E}}. \end{aligned} \quad (12)$$

Here, $\mathbf{m}^{\text{chir}} = \frac{d}{2}\Delta\mathbf{j} \times \mathbf{z}$ represents the in-plane magnetic density. The chiral nature of the responses characterized by σ^{chir} become more apparent in Eq. (12).

For a 2D bilayer featuring 180°-rotation symmetry around the y axis at the middle point between the two layers, we have $H^{(1)}(M_{yz}\mathbf{k}) = H^{(2)}(\mathbf{k})$, $H^{(2)}(M_{yz}\mathbf{k}) = H^{(1)}(\mathbf{k})$, and $H^{(i)}(M_{yz}\mathbf{k}) = H^{(i)}(\mathbf{k})$, where M_{yz} is the operator: $M_{yz}(k_x, k_y) = (-k_x, k_y)$. One can obtain $v_x^{(1)}(M_{yz}\mathbf{k}) = -v_x^{(2)}(\mathbf{k})$, $v_y^{(1)}(M_{yz}\mathbf{k}) = v_y^{(2)}(\mathbf{k})$, $v_x^{(i)}(M_{yz}\mathbf{k}) = -v_x^{(i)}(\mathbf{k})$, and $v_y^{(i)}(M_{yz}\mathbf{k}) = v_y^{(i)}(\mathbf{k})$. Therefore, we can get $\sigma_{16} = -\sigma_{36}$, i.e., $\sigma'_{xy} + \tilde{\sigma}'_{xy} = -(\sigma''_{xy} + \tilde{\sigma}''_{xy})$. Furthermore, if the bilayer also exhibits rotational invariance around the z axis, we can derive $\tilde{\sigma}'_{xy} = \tilde{\sigma}''_{xy} = 0$ as well, resulting in $\sigma'_{xy} = -\sigma''_{xy}$. Consequently, this allows us to deduce $\sigma^{\text{chir}} = \sigma_{xy} + \sigma'_{xy}$ and $D_{\text{chir}} = D_{xy} + D'_{xy}$, aligning with the chiral Drude parameter discussed in Ref. [19].

IV. RELATION BETWEEN σ^{chir} AND CD

We now examine the scattering behavior when the bilayer is subjected to linearly polarized light $\mathbf{E}_i = (E_i^x \mathbf{e}_x + E_i^y \mathbf{e}_y)e^{iqz}$ ($q = \omega/c$), as depicted in Fig. 1(a). We consider the scenario where the bilayer is in contact with a substrate having a dielectric constant ε and occupying the half-space ($z > d$), while the remaining half-space ($z < 0$) is vacuum. In the absence of currents, we can determine the electric fields by applying the boundary conditions of Maxwell's equations at the interface ($z = d$). Consequently, we derive the reflection wave $\mathbf{E}_r^0 = (E_r^{0,x} \mathbf{e}_x + E_r^{0,y} \mathbf{e}_y)e^{-iqz}$ and transmission wave $\mathbf{E}_t^0 = (E_t^{0,x} \mathbf{e}_x + E_t^{0,y} \mathbf{e}_y)e^{iqz}$ ($q' = \omega\sqrt{\varepsilon}/c$), wherein $E_r^{0,\alpha} = r_0 e^{i2qd} E_i^\alpha$ and $E_t^{0,\alpha} = t_0 e^{i(q-q')d} E_i^\alpha$ ($\alpha = x, y$), with

$$r_0 = \frac{1 - \sqrt{\varepsilon}}{1 + \sqrt{\varepsilon}}, \quad t_0 = 1 + r_0. \quad (13)$$

The currents within the bilayers can be deduced from the constitutive equation $\mathbf{j} = \sigma^{\text{BL}}\mathbf{E}^0$. Notably, these currents are of the first order with respect to optical conductivity σ_{ij} . The high-order terms of σ_{ij} can be safely neglected

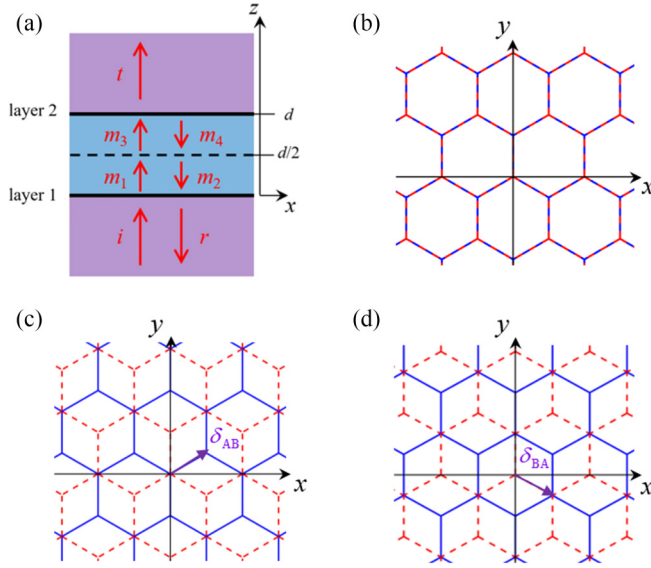


FIG. 1. (a) Schematic of the electromagnetic scattering at a bilayer. The two layers are located at $z = 0$ and $z = d$ planes, and the interlayer current is assumed to locate at the $z = d/2$ plane. i , r , and t represent the incident, reflected, and transmitted waves, respectively. The electromagnetic waves which propagate between two layers are represented by m_1 – m_4 . (b)–(d) Three typical stacking patterns of bilayer graphene, which are AA, AB, and BA, respectively.

under the condition where $\sigma_{ij}/(c\epsilon_0) \ll 1$. The total electric field \mathbf{E} is given as $\mathbf{E} = \mathbf{E}_0 + \mathbf{E}^{\text{ind}}$, where \mathbf{E}^{ind} represents the electric field induced by currents $\mathbf{j} = [\mathbf{j}^{(1)}; \mathbf{j}^{(2)}; \mathbf{j}^{(i)}]$. For the sake of simplification, we assume that the interlayer current is confined in the middle plane ($z = d/2$) between the two monolayers.

The induced electric fields can be resolved through the application of the boundary conditions of Maxwell's equations,

which gives [34]

$$\begin{aligned} \mathbf{E}_t^{\text{ind}} &= -\frac{t_0}{2\epsilon_0 c} [e^{i(q-q')d} \mathbf{j}^{(1)} + e^{-iq'd} \mathbf{j}^{(2)} + e^{i(1/2q-q')d} \mathbf{j}^{(i)}] e^{iq'z}, \\ \mathbf{E}_r^{\text{ind}} &= -\frac{1}{2\epsilon_0 c} [(1 + r_0 e^{i2qd}) \mathbf{j}^{(1)} + t_0 e^{iqd} \mathbf{j}^{(2)} \\ &\quad + (1 + r_0 e^{iqd}) e^{i(qd/2)} \mathbf{j}^{(i)}] e^{-iqz}. \end{aligned} \quad (14)$$

Subsequently, we derive the transmission wave $\mathbf{E}_t = \mathbf{E}_t^0 + \mathbf{E}_t^{\text{ind}} = (E_t^x \mathbf{e}_x + E_t^y \mathbf{e}_y) e^{iq'z}$ and reflection waves $\mathbf{E}_r = \mathbf{E}_r^0 + \mathbf{E}_r^{\text{ind}} = (E_r^x \mathbf{e}_x + E_r^y \mathbf{e}_y) e^{-iqz}$. The transmission and reflection amplitudes $t_{\alpha\beta}$ and $r_{\alpha\beta}$ are given by the linear relationship:

$$\begin{pmatrix} E_t^x \\ E_t^y \end{pmatrix} = \begin{pmatrix} t_{xx} & t_{xy} \\ t_{yx} & t_{yy} \end{pmatrix} \begin{pmatrix} E_i^x \\ E_i^y \end{pmatrix}, \quad (15)$$

and

$$\begin{pmatrix} E_r^x \\ E_r^y \end{pmatrix} = \begin{pmatrix} r_{xx} & r_{xy} \\ r_{yx} & r_{yy} \end{pmatrix} \begin{pmatrix} E_i^x \\ E_i^y \end{pmatrix}, \quad (16)$$

which are presented in the Supplemental Material [34]. CPL has the electric fields of $(\mathbf{e}_x \pm i\mathbf{e}_y)/\sqrt{2}$. The amplitudes of the transmission and reflection waves given by using Eqs. (15) and (16) are, respectively:

$$\begin{aligned} \mathbf{t}_{\pm} &= \frac{1}{\sqrt{2}} [(t_{xx} \pm it_{xy}) \mathbf{e}_x + (t_{yx} \pm it_{yy}) \mathbf{e}_y], \\ \mathbf{r}_{\pm} &= \frac{1}{\sqrt{2}} [(r_{xx} \pm ir_{xy}) \mathbf{e}_x + (r_{yx} \pm ir_{yy}) \mathbf{e}_y]. \end{aligned} \quad (17)$$

The absorption efficiencies A_{\pm} of the bilayer to the right- and left-CPL can be determined from $A_{\pm} = 1 - R_{\pm} - T_{\pm}$, where $R_{\pm} = |\mathbf{r}_{\pm}|^2$ and $T_{\pm} = \sqrt{\epsilon} |\mathbf{t}_{\pm}|^2$ represent the reflection and transmission coefficients, respectively. Assuming $qd \ll 1$ and $\sigma_{ij}/(c\epsilon_0) \ll 1$, the CD is given as

$$\text{CD} \approx -\frac{2\omega d}{c} \frac{\sqrt{\epsilon} \text{Re}[\sigma_{xy} + \frac{1}{2}\sigma'_{xy} - \frac{1}{2}(1 - \frac{1}{2}r_0)\sigma''_{xy}] + \frac{t_0^2}{4t_0} \text{Re}[\sigma'_{xy} + \sigma''_{xy}]}{\text{Re}(\sigma_{xx}^{\text{eff}} + \sigma_{yy}^{\text{eff}})}, \quad (18)$$

where we only consider the lowest orders of qd and σ_{ij} . For $\epsilon = 1$, we can obtain $r_0 = 0$ and $t_0 = 1$. The CD further becomes

$$\text{CD} \approx -\frac{2\omega d}{c} \frac{\text{Re}\sigma_{\text{chir}}}{\text{Re}(\sigma_{xx}^{\text{eff}} + \sigma_{yy}^{\text{eff}})}. \quad (19)$$

The expressions for σ_{xx}^{eff} and σ_{yy}^{eff} are presented in the Supplemental Material [34]. It is evident that the presence of $\text{Re}\sigma_{\text{chir}} \neq 0$ is necessary for the generation of nonzero CD signals when the bilayer is suspended in vacuum, thereby highlighting that the chiral response of a bilayer with TRS can be generally characterized by $\sigma_{\text{chir}} \neq 0$. As a special case, the continuum model of TBG has $\sigma'_{xy} = \sigma''_{xy} = 0$ because the interlayer transitions are independent of wave vector [6], and the interlayer current is thus neglectable. The CD of TBG given by Eq. (18) is consistent with that reported in the previous literature [16]. While the CD has been explored

extensively for TBG through a series of theoretical investigations [15,17,18], the methodologies established in these studies can also be adopted for numerical calculation of CD in various other bilayer configurations. Nevertheless, a direct CD expression tailored for bilayers with TRS remains absent. The equation [Eq. (18)] introduced herein holds valuable potential for CD prediction in bilayer systems with TRS. Its practical applicability can be further bolstered through experimental validation.

V. SYMMETRY-DEPENDENT σ_{chir}

We now tend to the relationship between the chiral response in a bilayer and the underlying lattice symmetries, including mirror and spatial inversion symmetries. Previous researchers have suggested that the chiral response in a TBG system is attributed to the lack of mirror symmetry resulting from the twist operation applied between the two graphene

monolayers [16]. In a bilayer system, the mirror operation with respect to the x - y plane M_{xy} results in the exchange of the two atomic layers, while the wave vector remains unchanged. Therefore, the mirror symmetry with respect to the x - y plane leads to $\mathbf{v}_x^{(1)}(\mathbf{k}) = \mathbf{v}_x^{(2)}(\mathbf{k})$ and $\mathbf{v}_y^{(1)}(\mathbf{k}) = \mathbf{v}_y^{(2)}(\mathbf{k})$. Using Eq. (4), we have $\sigma_{14} = \sigma_{23}$, $\sigma_{16} = \sigma_{36}$, and $\sigma_{25} = \sigma_{45}$, which results in $\sigma_{xy} = 0$, $\sigma'_{xy} = \sigma''_{xy}$, and thereby $\sigma_{\text{chir}} = 0$. Similarly, for the mirror operation with respect to the x - z plane, M_{xz} , the wave vector \mathbf{k} becomes $M_{xz}\mathbf{k}$, while the atomic layers remain unchanged. The mirror symmetry with respect to the x - z plane in a bilayer system results in $\mathbf{v}_x^{(\alpha)}(\mathbf{k}) = \mathbf{v}_x^{(\alpha)}(M_x\mathbf{k})$ and $\mathbf{v}_y^{(\alpha)}(\mathbf{k}) = -\mathbf{v}_y^{(\alpha)}(M_x\mathbf{k})$, with $\alpha \in 1, 2$, inter, which leads to $\sigma_{14} = \sigma_{23} = 0$, $\sigma_{16} = \sigma_{25} = 0$, and $\sigma_{36} = \sigma_{45} = 0$, according to Eq. (4), and thereby $\sigma_{\text{chir}} = 0$. The mirror symmetry with respect to other planes containing the z axis will also lead to $\sigma_{\text{chir}} = 0$ because σ_{chir} is rotationally invariant. Therefore, to produce a chiral response, it is necessary to eliminate all mirror symmetries in a bilayer system. Moreover, spatial inversion symmetry should also be removed from the bilayer system to achieve a chiral response. Under spatial inversion symmetry, the velocity operators satisfy $\mathbf{v}_{x,(y)}^{(1)}(\mathbf{k}) = -\mathbf{v}_{x,(y)}^{(2)}(-\mathbf{k})$ and $\mathbf{v}_{x,(y)}^{(\text{inter})}(\mathbf{k}) = -\mathbf{v}_{x,(y)}^{(\text{inter})}(-\mathbf{k})$, which engenders $\sigma_{14} = \sigma_{23}$, $\sigma_{16} = \sigma_{36}$, and $\sigma_{25} = \sigma_{45}$, according to Eq. (4), and thereby an achiral response with $\sigma_{\text{chir}} = 0$.

VI. CHIRAL PLASMONS IN A 2D BILAYER

Plasmon modes refer to the electromagnetic fields arising from the collective oscillations of electrons. Notably, the transverse component of the Poynting vectors has recently emerged as a reliable means of characterizing plasmon chirality [30,31]. In the subsequent section, we delve into the exploration of chirality of plasmons with a 2D bilayer by considering the influence of the interlayer current.

In the context of a 2D bilayer, we assume the plasmon currents for layer 1 [$\mathbf{j}^{(1)}$] and layer 2 [$\mathbf{j}^{(2)}$] are localized at the $z = 0$ and $z = d$ planes, respectively. The interlayer current $\mathbf{j}^{(i)}$ is assumed to be confined in the middle plane ($z = d/2$). We further posit that the bilayer is surrounded by a medium characterized by a dielectric constant ε and magnetic permeability $\mu = 1$. The current $\mathbf{j}^{(\alpha)}$ [$\alpha \in (1, 2, i)$] is defined as $\mathbf{j}^{(\alpha)} = [j_{\parallel}^{(\alpha)}\mathbf{e}_q + j_{\perp}^{(\alpha)}\mathbf{e}_{q,\perp}]$, where \mathbf{q} is the wave vector of plasmon, \mathbf{e}_q and $\mathbf{e}_{q,\perp}$ represent unit vectors that align parallel and perpendicular to the wave vector \mathbf{q} , respectively. It is noteworthy that the phase factor $e^{i(\mathbf{q}\cdot\mathbf{r}-\omega t)}$ is omitted in the expression of $\mathbf{j}^{(\alpha)}$. Within the half-space $z < 0$ or $z > d$, the electric and magnetic fields induced by currents $\mathbf{j}^{(\alpha)}$ can be expressed in the bases ($\mathbf{e}_q, \mathbf{e}_{q,\perp}, \mathbf{e}_z$) as

$$\mathbf{E}^{\text{ind},(\alpha)} = i\omega \begin{bmatrix} -d_l j_{\parallel}^{(\alpha)} \\ -d_l j_{\perp}^{(\alpha)} \\ -i \text{sgn}(z) q d_l j_{\parallel}^{(\alpha)} / q' \end{bmatrix} e^{i\mathbf{q}\cdot\mathbf{r}} e^{-q'|z-d_\alpha|}, \quad (20)$$

and

$$\mathbf{B}^{\text{ind},(\alpha)} = \begin{bmatrix} -\text{sgn}(z) q' d_l j_{\perp}^{(\alpha)} \\ -\text{sgn}(z) k_0^2 d_l j_{\parallel}^{(\alpha)} / q' \\ -i q d_l j_{\perp}^{(\alpha)} \end{bmatrix} e^{i\mathbf{q}\cdot\mathbf{r}} e^{-q'|z-d_\alpha|}. \quad (21)$$

Here, $q' = \sqrt{q^2 - \varepsilon \frac{\omega^2}{c^2}}$, $k_0 = \sqrt{\varepsilon} \frac{\omega}{c}$, $d_l = \frac{q'}{2\varepsilon\varepsilon_0\omega^2}$, and $d_t = -\frac{\mu_0}{2q'}$. Also, $z = d_\alpha$ is the plane where current $\mathbf{j}^{(\alpha)}$ is localized. Therefore, the total induced electric and magnetic fields are $\mathbf{E}^{\text{ind}} = \sum_\alpha \mathbf{E}^{\text{ind},(\alpha)}$ and $\mathbf{B}^{\text{ind}} = \sum_\alpha \mathbf{B}^{\text{ind},(\alpha)}$, respectively. The Poynting vector of the induced electromagnetic fields is defined by $\mathbf{P} = \frac{1}{2\mu_0} \text{Re}[(\mathbf{E}^{\text{ind}})^* \times \mathbf{B}^{\text{ind}}]$. In the limit of $q'd \ll 1$, we have

$$\mathbf{P} = \frac{1}{2\mu_0} \begin{pmatrix} P_{\parallel} \\ P_{\perp} \\ P_z \end{pmatrix} e^{-2q'|z|}, \quad (22)$$

where

$$\begin{aligned} P_{\parallel} &= \omega q \text{Re} \sum_{\alpha,\beta} [d_t^2 j_{\perp}^{(\alpha)*} j_{\perp}^{(\beta)} + d_t^2 k_0^2 j_{\parallel}^{(\alpha)*} j_{\parallel}^{(\beta)} / q'^2] \\ &\quad \times [1 + q' \text{sgn}(z)(d_\alpha + d_\beta)], \\ P_{\perp} &= -2\omega q d_l d_t \text{Re} \sum_{\alpha,\beta} j_{\parallel}^{(\alpha)*} j_{\perp}^{(\beta)} [1 + q' \text{sgn}(z)(d_\alpha + d_\beta)], \\ P_z &= i\omega \text{sgn}(z) \text{Re} \sum_{\alpha,\beta} [-d_t^2 k_0^2 j_{\parallel}^{(\alpha)*} j_{\parallel}^{(\beta)} / q' + q' d_t^2 j_{\perp}^{(\alpha)*} j_{\perp}^{(\beta)}] \\ &\quad \times [1 + q' \text{sgn}(z)(d_\alpha + d_\beta)]. \end{aligned} \quad (23)$$

The chiral plasmon is characterized by the nonzero transverse component of the Poynting vectors, i.e., $P_{\perp} \neq 0$. To gain insight into the origin of the chiral plasmon, it becomes imperative to establish a connection between the plasmon currents and the inherent attributes of bilayers, such as their optical conductivities. In the scope of this paper, we introduce the definitions of the plasmon current and electric field for the bilayer as $\mathbf{j}^{\text{BL}} = [\mathbf{j}^{(1)}; \mathbf{j}^{(2)}; \mathbf{j}^{(i)}]$ and $\mathbf{E}^{\text{BL}} = [\mathbf{E}^{(1)}; \mathbf{E}^{(2)}; \mathbf{E}^{(i)}]$, with $\mathbf{j}^{(\alpha)} = [j_{\parallel}^{(\alpha)}, j_{\perp}^{(\alpha)}]^T$ and $\mathbf{E}^{(\alpha)} = [E_{\parallel}^{(\alpha)}, E_{\perp}^{(\alpha)}]^T$. The linear response between current and electric field is written as $\mathbf{j}^{\text{BL}} = \boldsymbol{\sigma}^{\text{BL}} \mathbf{E}^{\text{BL}}$, where $\boldsymbol{\sigma}^{\text{BL}}$ is a 6×6 nonlocal response matrix for a finite wave vector \mathbf{q} . It is important to highlight that the matrix element $\sigma_{ij}(\mathbf{q}, \omega)$ does not necessarily equal $\sigma_{ji}(\mathbf{q}, \omega)$ even in bilayers with TRS, showcasing the intricate nature of nonlocal responses.

In the unretarded limit ($q \gg \sqrt{\varepsilon}\omega/c$), the bilayers exhibit support for two types of plasmon modes: an optical mode characterized by $\mathbf{e}_q \cdot \mathbf{E}^{(1)} = \mathbf{e}_q \cdot \mathbf{E}^{(2)}$ and an acoustic mode characterized by $\mathbf{e}_q \cdot \mathbf{E}^{(1)} = -\mathbf{e}_q \cdot \mathbf{E}^{(2)}$ [31]. Both modes fall within the longitudinal category, i.e. $\mathbf{e}_{q,\perp} \cdot \mathbf{E}^{(\alpha)} = 0$. In the context of bilayers featuring interlayer quantum coupling, it is typical for the attenuation factor of the Coulomb potential $e^{-q'd}$ to approximate 1. As a result, only the optical modes can be supported [34]. For instance, considering bilayer graphene with a carrier density of $n = 10^{12} \text{cm}^{-2}$ per layer and an interlayer distance of $d = 3.35 \text{Å}$, we can obtain $k_F d \approx 0.06$ and $e^{-k_F d} \approx 0.94$, where k_F represents the Fermi vector. Therefore, we will only focus on the optical plasmon modes in our subsequent analysis. For these optical plasmon modes, we have $E_{\parallel}^{(1)} = E_{\parallel}^{(2)} = E_{\parallel}^{(i)} = E$ and $E_{\perp}^{(\alpha)} = 0$. With these considerations, we can subsequently determine the plasmon currents and Poynting vectors.

For the sake of clarity, we will elucidate our points through two specific examples. First, in the limit of $d \rightarrow 0$, we have $P_{\perp} = \frac{\mu_0 q}{2\varepsilon\varepsilon_0\omega} \text{Re}[j_{\parallel}^{(\text{tot})*} j_{\perp}^{(\text{tot})}]$. Here, $j_{\parallel}^{(\text{tot})}$ and $j_{\perp}^{(\text{tot})}$

are the total transverse and longitudinal currents given by $j_{\parallel}^{(\text{tot})} = \sum_{\alpha} j_{\parallel}^{(\alpha)}$ and $j_{\perp}^{(\text{tot})} = \sum_{\alpha} j_{\perp}^{(\alpha)}$. In general, $j_{\parallel}^{(\text{tot})}$ is not equal to zero, a consequence of the density fluctuation of electrons inherent to plasmon modes. Here, $j_{\perp}^{(\text{tot})}$ can be expressed as $j_{\perp}^{(\text{tot})} = \sigma_{\perp q}(\mathbf{q}, \omega)E$, where $\sigma_{\perp q}(\mathbf{q}, \omega)$ is the total transverse component of optical conductivity matrix, given as $\sigma_{\perp q}(\mathbf{q}, \omega) = \sigma_{21} + \sigma_{23} + \sigma_{25} + \sigma_{41} + \sigma_{43} + \sigma_{45} + \sigma_{61} + \sigma_{63} + \sigma_{65}$. As a result, the chiral property of plasmons requires $\sigma_{\perp q}(\mathbf{q}, \omega) \neq 0$. The local response limit proves effective particularly for small wave vectors (for graphene, $q < k_F$), a range that aligns significantly with the experimental focuses. In the local response limit $\sigma_{ij}(\mathbf{q}, \omega) \approx \sigma_{ij}(\mathbf{q} \rightarrow 0, \omega)$, the transverse conductivity $\sigma_{\perp q}(\mathbf{q} \rightarrow 0, \omega)$ can manifest as nonzero within 2D systems where TRS is broken or in anisotropic 2D systems [34]. Therefore, to the zero order of interlayer distance d , P_{\perp} can be nonzero, and chiral plasmons can exist in these types of systems.

Secondly, for an isotropy 2D bilayer with TRS, in the local response limit, σ^{BL} can be written as

$$\sigma^{\text{BL}} = \begin{pmatrix} \sigma_{11} & 0 & \sigma_{13} & \sigma_{xy} & \sigma_{15} & \sigma'_{xy} \\ 0 & \sigma_{11} & -\sigma_{xy} & \sigma_{13} & -\sigma'_{xy} & \sigma_{15} \\ \sigma_{13} & -\sigma_{xy} & \sigma_{33} & 0 & \sigma_{35} & \sigma''_{xy} \\ \sigma_{xy} & \sigma_{13} & 0 & \sigma_{33} & -\sigma''_{xy} & \sigma_{35} \\ \sigma_{15} & -\sigma'_{xy} & \sigma_{35} & -\sigma''_{xy} & \sigma_{55} & 0 \\ \sigma'_{xy} & \sigma_{15} & \sigma''_{xy} & \sigma_{35} & 0 & \sigma_{55} \end{pmatrix}. \quad (24)$$

In this condition, $\sigma_{\perp q}(\mathbf{q}, \omega)$ is equal to zero. Consequently, P_{\perp} also attains zero value in the $d \rightarrow 0$ limit. However, using $\mathbf{j}^{\text{BL}} = \sigma^{\text{BL}}\mathbf{E}^{\text{BL}}$ and Eq. (23), we can get $P_{\perp} = \frac{\mu_0 q q' d}{2\epsilon\epsilon_0 \omega} \text{sgn}(z)|E|^2 \text{Re}(\sigma_{\text{chir}} \sigma_{\text{tot}}^*)$. Here, $\sigma_{\text{chir}} = \sigma_{xy} + \frac{1}{2}(\sigma'_{xy} - \sigma''_{xy})$ is the chiral optical conductivity introduced in previous section. Also, σ_{tot} is given as $\sigma_{\text{tot}} = \sigma_{11} + \sigma_{33} + \sigma_{55} + 2\sigma_{13} + 2\sigma_{15} + 2\sigma_{35}$, which generally stands apart from zero for plasmon modes. This observation enables us to infer that $\sigma_{\text{chir}} \neq 0$ leads to the emergence of nonzero P_{\perp} for plasmons within isotropic 2D systems with TRS. As a special case, $\sigma_{xy} \neq 0$ is an essential requirement for the manifestation of chiral plasmons within the continuum model of TBG [30,31].

In accordance with our theoretical framework, chiral plasmons, distinguished by the presence of a nonzero transverse component within the Poynting vectors, can be observed within specific contexts. These contexts encompass a 2D bilayer where TRS is lifted as well as anisotropic bilayers. Moreover, they also extend to isotropic bilayers where TRS is maintained and $\sigma_{\text{chir}} \neq 0$. It is worth highlighting that the nature of chiral plasmons differs from the chiral response previously discussed at $\mathbf{q} \rightarrow 0$. This distinction is particularly evident in the case of an anisotropic 2D bilayer, where chiral plasmons can manifest even in the presence of $\sigma_{\text{chir}} = 0$.

VII. CHIRAL RESPONSE IN UN-TBG

A highly symmetric bilayer graphene has three typical stacking patterns: AA, AB, BA, as shown in Figs. 1(b)–1(d), with the latter two patterns being energetically equivalent and more favorable than the first pattern. These three patterns

have mirror and spatial inversion symmetries and thereby achiral response. However, the mirror symmetries can be lifted by sliding one monolayer relative to another. Starting from AA stacking pattern, we define the sliding vector $\delta = m\mathbf{a}_1 + n\mathbf{a}_2$, where $\mathbf{a}_1 = \sqrt{3}a\mathbf{i}$ and $\mathbf{a}_2 = \sqrt{3}a/2\mathbf{i} + 3a/2\mathbf{j}$ are the basis vectors of graphene. Here, $\delta_{\text{AB}} = (\mathbf{a}_1 + \mathbf{a}_2)/3$ and $\delta_{\text{BA}} = (2\mathbf{a}_1 - \mathbf{a}_2)/3$ correspond to the AB and BA stacking patterns, respectively. Obviously, when the sliding vector is along the zigzag direction (\mathbf{a}_1 , \mathbf{a}_2 , or $\mathbf{a}_1 - \mathbf{a}_2$) or armchair direction ($\mathbf{a}_1 + \mathbf{a}_2$, $-\mathbf{2a}_1 + \mathbf{a}_2$, or $-\mathbf{a}_1 + \mathbf{2a}_2$), the mirror symmetries with respect to the plane containing the sliding vector and perpendicular to the x - y plane (basal plane) are preserved, and thus, the resulting bilayer graphene is achiral. For other sliding vectors, all the mirror symmetries are removed, but the spatial inversion symmetry remains intact. The spatial inversion symmetry of bilayer graphene can be lifted through the interaction with substrates [e.g., hexagonal boron nitride (h-BN) substrate] or by applying a bias voltage.

Without loss of generality, we consider the latter case to demonstrate the possibility of generate chiral response in un-TBG. We numerically calculate the intraband transition contribution to the chiral conductivity D_{chir} based on a TB model (see the Supplemental Material for details [34]). The D_{chir} contours of the bilayer graphene with the stacking pattern characterized by the sliding vector $\delta = x\mathbf{i} + y\mathbf{j}$, filling factor $\xi = 0.005$, and bias voltage $U = 0.1\text{eV}$ are plotted in Fig. 2(a). Here, $\xi = 1$ represents doping two electrons per unit cell. As a result, $\xi = 0.01$ corresponds to the electron density of $n = 3.8 \times 10^{13} \text{ cm}^{-2}$. For a certain δ , we can determine the atomic positions and establish the TB Hamiltonian. Diagonalizing the Hamiltonian allows us to obtain the energy eigenvalues and corresponding eigenstates. For a given filling factor ξ , we can derive the Fermi energy. Subsequently, the Drude matrix elements can be calculated using Eq. (5). The TB calculations demonstrate that the sliding vectors along the armchair or zigzag direction lead to $D_{\text{chir}}(\omega) = 0$, suggesting that bilayer graphene at these stacking patterns is achiral. This is consistent with the symmetry analysis. Moreover, we can find that $D_{\text{chir}}(-\delta, U) = D_{\text{chir}}(\delta, U)$. We attribute it to the symmetry operators that link the two stacking patterns. The stacking patterns of biased bilayer graphene characterized as δ and $-\delta$ but with identical U are connected through the use of mirror (M_{xy}) and spatial inversion (I) operators. Interestingly, $|D_{\text{chir}}(\omega)|$ reaches its maximal value at $\delta_{\text{W}_1} = (0.615\mathbf{i} + 0.639\mathbf{j}) \text{ \AA}$ (W_1 pattern) and $\delta_{\text{W}_2} = (1.845\mathbf{i} + 0.639\mathbf{j}) \text{ \AA}$ (W_2 pattern). The maximal value of $|D_{\text{chir}}(\omega)|$ is approximately on the order of $10^{-5}te^2/\hbar^2$, which is two orders of magnitude smaller than the values reported in TBG [37]. The electronic band structure of the biased bilayer graphene with W_1 stacking pattern is plotted in Fig. 2(b). Layer polarization is quite apparent, due to the interlayer charge transfer between two graphene layers induced by bias voltage. The filling factor dependence of D_{chir} corresponding to the two stacking patterns is plotted in Fig. 2(c). The two stacking patterns exhibit opposite D_{chir} for a specific ξ . The Drude matrix elements D_{xy} , D'_{xy} , and D''_{xy} exhibit opposite trends for the two stacking patterns, as illustrated in Figs. 2(d) and 2(e). Unlike the findings in TBG [19], $D'_{xy} \neq -D''_{xy}$ is obtained in these two stacking patterns due to the reduced symmetries. We also plotted the bias voltage dependence of D_{chir} corresponding to the two

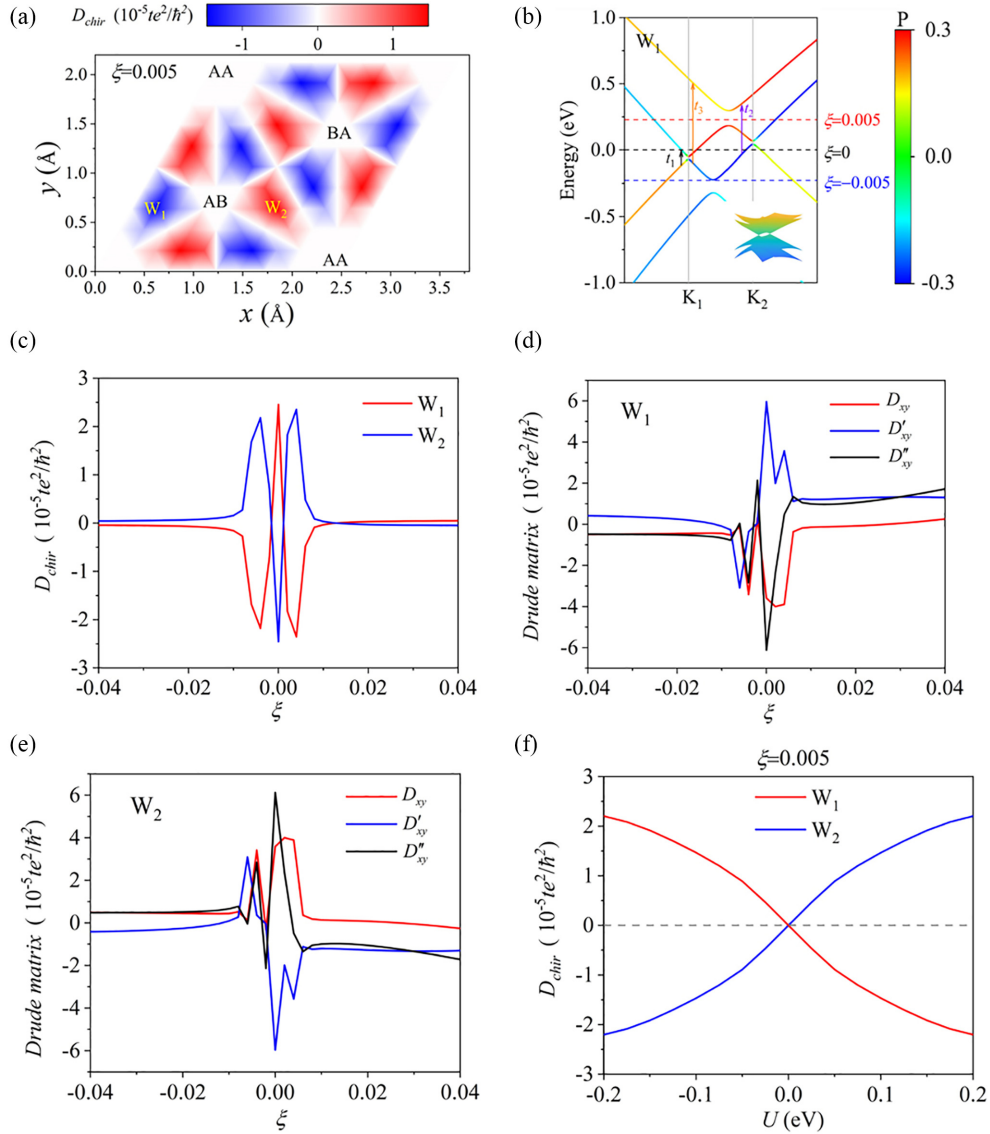


FIG. 2. (a) D_{chir} as a function of the slipping vector $\delta = xi\mathbf{i} + y\mathbf{j}$ between two graphene layers for biased bilayer graphene with $U = 0.1$ eV and $\xi = 0.005$. D_{chir} is in units of $10^{-5}te^2/\hbar^2$, where $t = 2.7\text{eV}$. (b) The layer-polarized band structure for biased bilayer graphene of W_1 pattern with $U = 0.1\text{eV}$. K_1 and K_2 represent two maximum points of the second energy band, which is shown more clearly in the three-dimensional (3D) band structures. The Fermi energy for different filling factors and several electronic transition processes (t_1 , t_2 , and t_3) are also shown. (c) D_{chir} as a function of ξ for biased bilayer graphene with $U = 0.1$ eV of W_1 and W_2 patterns, respectively. The filling dependence of D_{xy} , D'_{xy} , and D''_{xy} for W_1 and W_2 patterns are plotted in (d) and (e), respectively. (f) D_{chir} as the function of U for biased bilayer graphene with $\xi = 0.005$ of W_1 and W_2 patterns, respectively.

stacking patterns for a filling factor $\xi = 0.005$ in Fig. 2(f). It is noteworthy that the D_{chir} values for bilayer graphene with identical sliding vector but opposite bias voltages exhibit opposite behavior, specifically $D_{\text{chir}}(\delta, -U) = -D_{\text{chir}}(\delta, U)$, since they are connected through the spatial inversion operator. The D_{chir} is equal to zero for $U = 0$ due to the presence of spatial inversion symmetry, aligning with our symmetry analysis.

Figures 3(a) and 3(b) showcase the real part of σ_{chir} and CD computed using Eq. (19) for $U = 0.1\text{eV}$ and stacking pattern W_1 . It is worthy highlighting that the peaks observed in both $\text{Re}\sigma_{\text{chir}}$ and CD agree well with the energies of certain electron transition processes indicated in the band structures presented in Fig. 2(b). In this analysis, our focus is solely

on $\xi = 0$. The t_1 represents the interband transition processes with the minimum transition energies, while t_2 and t_3 represent the interband transitions involving nested energy bands. Figures 3(c) and 3(d) illustrate the comparison of $\text{Re}\sigma_{\text{chir}}$ and CD among distinct stacking patterns of biased bilayer graphene. Our chosen parameters are $U = 0.2$ eV and $\xi = 0.0175$ ($n = 6.65 \times 10^{13} \text{cm}^{-2}$), values that align with experimental feasibility [38]. Stacking patterns W_1 and W_2 exhibit nonzero $\text{Re}\sigma_{\text{chir}}$ and CD across a wide frequency range, whereas the nonchiral stacking pattern W_3 (with $\delta_{W_3} = 0.639\text{\AA}j$) yields nearly negligible $\text{Re}\sigma_{\text{chir}}$ and CD. The chiral response can be enhanced when the bilayer graphene is placed on a hBN substrate, as simulated by adding the additional on-site energies for atoms of one layer [34]. For the W_1 stacking pattern on a

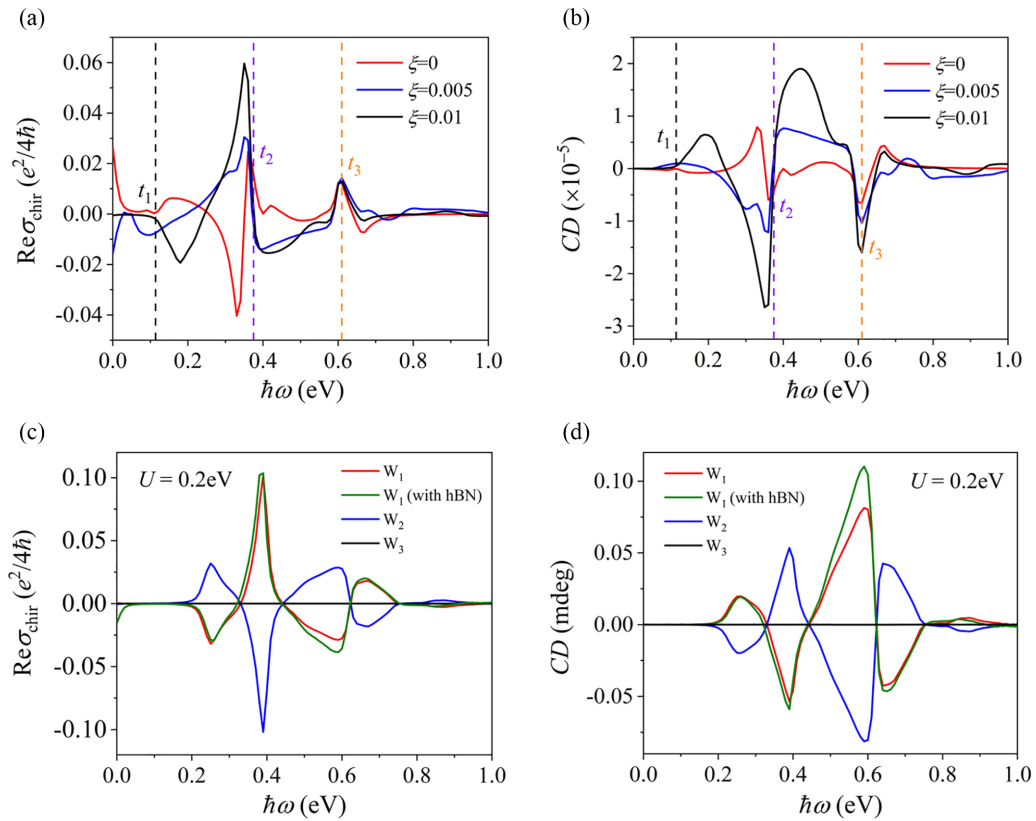


FIG. 3. (a) The real part of σ_{chir} as a function of energy $\hbar\omega$ for biased bilayer graphene of W_1 pattern with $U = 0.1$ eV. The corresponding circular dichroism (CD) for $\varepsilon = 1$ is shown in (b). (c) The real part of σ_{chir} for biased bilayer graphene of W_1 pattern, W_1 pattern with hBN substrate, W_2 pattern, and W_3 pattern, respectively. We have taken $U = 0.2$ eV and $\xi = 0.0175$. The corresponding CD is shown in (d).

hBN substrate, the maximum CD value reaches ~ 0.1 mdeg, akin to the order of magnitude observed in small-twist-angle TBG [16]. Experimental observations indicate CD values in the range of a few mdeg for large-twist-angle TBG ($\theta \geq 14^\circ$) [14], a range consistent with CD magnitudes observed in various chiral molecules [39]. It is worth noting that employing superchiral light can elevate the asymmetry absorption factor by an order of magnitude [40]. Thus, experiments have the potential to unveil the chiral response of biased bilayer graphene with interlayer sliding through the utilization of superchiral light. Importantly, the chiral characteristic σ_{chir} offers a means to assess and anticipate the intrinsic chirality of diverse 2D bilayers possessing TRS.

VIII. CONCLUSIONS

In summary, we propose a universal criterion for generation of chiral response in a 2D bilayer without the need of breaking TRS. We introduce chiral conductivity $\sigma_{\text{chir}} = \sigma_{xy} + \frac{1}{2}\sigma'_{xy} - \frac{1}{2}\sigma''_{xy}$ and demonstrate that $\sigma_{\text{chir}} \neq 0$ features a chiral response of a 2D bilayer. This criterion is more univer-

sal than that ($\sigma_{xy} \neq 0$) developed for TBGs. According to this criterion, to achieve a chiral response in the 2D bilayers while preserving TRS, it is necessary to remove both the mirror and spatial inversion symmetries. We also set up an analytic relation between CD and σ_{chir} , which will be quite useful for evaluating CD of a 2D bilayer. Furthermore, our investigation extends to the examination of chirality in plasmons within 2D bilayers. Our finding indicates the presence of chiral plasmons in 2D bilayers where TRS is broken as well as in anisotropic bilayers. Additionally, these chiral plasmons can manifest in isotropic bilayers that possess both TRS and $\sigma_{\text{chir}} \neq 0$. Taking the un-TBG under a bias voltage as a demo system, we verify the criterion by numerical calculations. The findings establish a comprehensive theoretical framework for exploring chiral responses in 2D bilayer systems.

ACKNOWLEDGMENTS

This paper is supported by the National Natural Science Foundation of China (No. 12074218) and the Taishan Scholar Program of Shandong Province.

- [1] M. B. Smith and J. March, *March's Advanced Organic Chemistry: Reactions, Mechanisms and Structure* (John Wiley & Sons, Inc., Hoboken, 2007).
 [2] Y. Inoue and V. Ramamurthy, *Chiral Photochemistry* (Taylor & Francis Group LLC, Boca Raton, 2004).

- [3] Y. Zhao, A. N. Askarpour, L. Sun, J. Shi, X. Li, and A. Alu, Chirality detection of enantiomers using twisted optical metamaterials, *Nat. Commun.* **8**, 14180 (2017).
 [4] B. Göhler, V. Hamelbeck, T. Z. Markus, M. Kettner, G. F. Hanne, Z. Vager, R. Naaman, and H. Zacharias, Spin selectivity

- in electron transmission through self-assembled monolayers of double-stranded DNA, *Science* **331**, 894 (2011).
- [5] W. F. Koehl, M. H. Wong, C. Poblenz, B. Swenson, U. K. Mishra, J. S. Speck, and D. D. Awschalom, Current-induced spin polarization in gallium nitride, *Appl. Phys. Lett.* **95**, 072110 (2009).
- [6] R. Bistritzer and A. H. MacDonald, Moire bands in twisted double-layer graphene, *Proc. Natl. Acad. Sci. USA* **108**, 12233 (2011).
- [7] C. J. Tabert and E. J. Nicol, Dynamical conductivity of AA-stacked bilayer graphene, *Phys. Rev. B* **86**, 075439 (2012).
- [8] E. J. Nicol and J. P. Carbotte, Optical conductivity of bilayer graphene with and without an asymmetry gap, *Phys. Rev. B* **77**, 155409 (2008).
- [9] L. Wang, E. M. Shih, A. Ghiotto, L. Xian, D. A. Rhodes, C. Tan, M. Claassen, D. M. Kennes, Y. Bai, B. Kim *et al.*, Correlated electronic phases in twisted bilayer transition metal dichalcogenides, *Nat. Mater.* **19**, 861 (2020).
- [10] E. C. Regan, D. Wang, C. Jin, M. I. Bakti Utama, B. Gao, X. Wei, S. Zhao, W. Zhao, Z. Zhang, K. Yumigeta *et al.*, Mott and generalized Wigner crystal states in WSe_2/WS_2 moire superlattices, *Nature (London)* **579**, 359 (2020).
- [11] D. L. Miller, K. D. Kubista, G. M. Rutter, M. Ruan, W. A. de Heer, P. N. First, and J. A. Stroscio, Structural analysis of multilayer graphene via atomic moiré interferometry, *Phys. Rev. B* **81**, 125427 (2010).
- [12] A. Luican, G. Li, A. Reina, J. Kong, R. R. Nair, K. S. Novoselov, A. K. Geim, and E. Y. Andrei, Single-layer Behavior and Its Breakdown in Twisted Graphene Layers, *Phys. Rev. Lett.* **106**, 126802 (2011).
- [13] G. Li, A. Luican, J. M. B. Lopes dos Santos, A. H. Castro Neto, A. Reina, J. Kong, and E. Y. Andrei, Observation of Van Hove singularities in twisted graphene layers, *Nat. Phys.* **6**, 109 (2009).
- [14] C. J. Kim, A. Sanchez-Castillo, Z. Ziegler, Y. Ogawa, C. Noguez, and J. Park, Chiral atomically thin films, *Nat. Nanotechnol.* **11**, 520 (2016).
- [15] E. Suárez Morell, L. Chico, and L. Brey, Twisting Dirac fermions: Circular dichroism in bilayer graphene, *2D Mater.* **4**, 035015 (2017).
- [16] T. Stauber, T. Low, and G. Gomez-Santos, Chiral Response of Twisted Bilayer Graphene, *Phys. Rev. Lett.* **120**, 046801 (2018).
- [17] S. T. Ho and V. N. Do, Optical activity and transport in twisted bilayer graphene: Spatial dispersion effects, *Phys. Rev. B* **107**, 195141 (2023).
- [18] K. Chang, Z. Zheng, J. E. Sipe, and J. L. Cheng, Theory of optical activity in doped systems with application to twisted bilayer graphene, *Phys. Rev. B* **106**, 245405 (2022).
- [19] T. Stauber, T. Low, and G. Gómez-Santos, Linear response of twisted bilayer graphene: Continuum versus tight-binding models, *Phys. Rev. B* **98**, 195414 (2018).
- [20] A. Guerrero-Martinez, B. Auguie, J. L. Alonso-Gomez, Z. Dzolic, S. Gomez-Grana, M. Zinic, M. M. Cid, and L. M. Liz-Marzan, Intense optical activity from three-dimensional chiral ordering of plasmonic nanoantennas, *Angew. Chem., Int. Ed.* **50**, 5499 (2011).
- [21] X. Shen, A. Asenjo-Garcia, Q. Liu, Q. Jiang, F. J. Garcia de Abajo, N. Liu, and B. Ding, Three-dimensional plasmonic chiral tetramers assembled by DNA origami, *Nano Lett.* **13**, 2128 (2013).
- [22] A. Kuzyk, R. Schreiber, Z. Fan, G. Pardatscher, E. M. Röller, A. Hoge, F. C. Simmel, A. O. Govorov, and T. Liedl, DNA-based self-assembly of chiral plasmonic nanostructures with tailored optical response, *Nature (London)* **483**, 311 (2012).
- [23] B. Yeom, H. Zhang, H. Zhang, J. I. Park, K. Kim, A. O. Govorov, and N. A. Kotov, Chiral plasmonic nanostructures on achiral nanopillars, *Nano Lett.* **13**, 5277 (2013).
- [24] M. Hentschel, M. Schäferling, X. Duan, H. Giessen, and N. Liu, Chiral Plasmonics, *Sci. Adv.* **3**, e1602735 (2017).
- [25] H. E. Lee, H. Y. Ahn, J. Mun, Y. Y. Lee, M. Kim, N. H. Cho, K. Chang, W. S. Kim, J. Rho, and K. T. Nam, Amino-acid- and peptide-directed synthesis of chiral plasmonic gold nanoparticles, *Nature (London)* **556**, 360 (2018).
- [26] X. Yin, M. Schaferling, A. K. Michel, A. Tittl, M. Wuttig, T. Taubner, and H. Giessen, Active chiral plasmonics, *Nano Lett.* **15**, 4255 (2015).
- [27] Q. Zhang, T. Hernandez, K. W. Smith, S. A. Hosseini Jebeli, A. X. Dai, L. Warning, R. Baiyasi, L. A. McCarthy, H. Guo, D. H. Chen *et al.*, Unraveling the origin of chirality from plasmonic nanoparticle-protein complexes, *Science* **365**, 1475 (2019).
- [28] J. C. Song and M. S. Rudner, Chiral plasmons without magnetic field, *Proc. Natl. Acad. Sci. USA* **113**, 4658 (2016).
- [29] A. Kumar, A. Nemilentsau, K. H. Fung, G. Hanson, N. X. Fang, and T. Low, Chiral plasmon in gapped Dirac systems, *Phys. Rev. B* **93**, 041413(R) (2016).
- [30] T. Stauber, T. Low, and G. Gomez-Santos, Plasmon-enhanced near-field chirality in twisted van der Waals heterostructures, *Nano Lett.* **20**, 8711 (2020).
- [31] T. Stauber, M. Wackerl, P. Wenk, D. Margetis, J. González, G. Gómez-Santos, and J. Schliemann, Neutral magic-angle bilayer graphene: Condon instability and chiral resonances, *Small Sci.* **3**, 2200080 (2023).
- [32] S. A. Mikhailov and K. Ziegler, New Electromagnetic Mode in Graphene, *Phys. Rev. Lett.* **99**, 016803 (2007).
- [33] Z. Addison, J. Park, and E. J. Mele, Twist, slip, and circular dichroism in bilayer graphene, *Phys. Rev. B* **100**, 125418 (2019).
- [34] See Supplemental Material at <http://link.aps.org/supplemental/10.1103/PhysRevB.108.125415> for the demonstration of rotationally invariant chiral conductivity of 2D monolayer, the achiral response matrices, the transmission and reflection amplitudes, the theory for plasmon in a 2D bilayer, the TB model of bilayer graphene, and the computational details. This contains references to T. Stauber and G. Gomez-Santos, Plasmons in layered structures including graphene, *New J. Phys.* **14**, 105018 (2012); P. Moon and M. Koshino, Optical absorption in twisted bilayer graphene, *Phys. Rev. B* **87**, 205404 (2013); Y.-H. Zhang, D. Mao, and Th. Senthil, Twisted bilayer graphene aligned with hexagonal boron nitride: Anomalous Hall effect and a lattice model, *Phys. Rev. Res.* **1**, 033126 (2019).
- [35] W. Yao, D. Xiao, and Q. Niu, Valley-dependent optoelectronics from inversion symmetry breaking, *Phys. Rev. B* **77**, 235406 (2008).
- [36] D. Xiao, G. B. Liu, W. Feng, X. Xu, and W. Yao, Coupled Spin and Valley Physics in Monolayers of MoS_2 and Other Group-VI Dichalcogenides, *Phys. Rev. Lett.* **108**, 196802 (2012).

- [37] T. Stauber, J. González, and G. Gómez-Santos, Change of chirality at magic angles of twisted bilayer graphene, *Phys. Rev. B* **102**, 081404(R) (2020).
- [38] T. Ohta, A. Bostwick, T. Seyller, K. Horn, and E. Rotenberg, Controlling the electronic structure of bilayer graphene, *Science* **313**, 951 (2006).
- [39] S. M. Kelly, T. J. Jess, and N. C. Price, How to study proteins by circular dichroism, *Biochim. Biophys. Acta* **1751**, 119 (2005).
- [40] Y. Tang and A. E. Cohen, Enhanced enantioselectivity in excitation of chiral molecules by superchiral light, *Science* **332**, 333 (2011).